Local stabilisation of polar order at charged antiphase boundaries in antiferroelectric (Bi0.85Nd0.15)(Ti0.1Fe0.9)O3

Ian MacLaren, LiQiu Wang, Owen Morris, Alan J. Craven, Robert L. Stamps et al.

Citation: APL Mater. **1**, 021102 (2013); doi: 10.1063/1.4818002
View online: http://dx.doi.org/10.1063/1.4818002
View Table of Contents: http://aplmaterials.aip.org/resource/1/AMPADS/v1/i2
Published by the AIP Publishing LLC.

Local stabilisation of polar order at charged antiphase boundaries in antiferroelectric $(Bi_{0.85}Nd_{0.15})(Ti_{0.1}Fe_{0.9})O_3$

Ian MacLaren,[1,2,a] LiQiu Wang,[1] Owen Morris,[1] Alan J. Craven,[1,2] Robert L. Stamps,[1] Bernhard Schaffer,[1,2] Quentin M. Ramasse,[2] Shu Miao,[3] Kambiz Kalantari,[3] Iasmi Sterianou,[3] and Ian M. Reaney[3]
[1]*SUPA School of Physics and Astronomy, University of Glasgow, Glasgow G12 8QQ, United Kingdom*
[2]*SuperSTEM Laboratory, SciTech Daresbury, Keckwick Lane, Warrington WA4 4AD, United Kingdom*
[3]*Department of Materials Science and Engineering, University of Sheffield, Mappin St, Sheffield, S1 3JD, United Kingdom*

(Received 8 March 2013; accepted 9 May 2013; published online 13 August 2013)

Observation of an unusual, negatively-charged antiphase boundary in $(Bi_{0.85}Nd_{0.15})(Ti_{0.1}Fe_{0.9})O_3$ is reported. Aberration corrected scanning transmission electron microscopy is used to establish the full three dimensional structure of this boundary including O-ion positions to $\sim\pm10$ pm. The charged antiphase boundary stabilises tetragonally distorted regions with a strong polar ordering to either side of the boundary, with a characteristic length scale determined by the excess charge trapped at the boundary. Far away from the boundary the crystal relaxes into the well-known Nd-stabilised antiferroelectric phase. [http://dx.doi.org/10.1063/1.4818002]

Structural responses to interfaces and impurities can enable new functionalities in ferroic oxides. Examples of surprising interface phenomena include conductive domain boundaries,[1] the suppression of polarisation at charged domain walls in ferroelectrics,[2] charge compensation at epitaxial heterointerfaces between a ferroelectric oxide and a non-ferroelectric oxide,[3] and the emergence of novel electronic states at the interface of two oxides resulting in interfacial conductivity[4,5] or local magnetic orderings.[6] In the present paper, it is shown that an unusual and strongly charged kind of antiphase boundary (APB) forms in $(Bi_{0.85}Nd_{0.15})(Ti_{0.1}Fe_{0.9})O_3$. This boundary is defined by a highly distorted region a few unit cells in thickness in which a pseudotetragonal polar-ordered phase is stabilised in preference to the antiferroelectric matrix, with the peak in spontaneous polarization occurring at the boundary edges.

Understanding the structural origins of these phenomena requires detailed knowledge of atomic scale features. Detailed studies of interfaces in perovskite oxides have been made possible by imaging and quantification of polarisation using advanced high-resolution electron microscopy[2,3,7–14]; this has generally proceeded by measuring the displacement of one or more atoms in the unit cell from their positions in an unpolarised perovskite and then calculating the polarisation on a cell-by-cell basis. These advanced techniques have been used in previous studies[3,8,13,14] to validate models of interfacial polar behaviour, including semi-classical and first-principles quantum mechanical models of polarization compensation that have yielded new insights into polarisation behaviour at the atomic scale.

ATOMIC RESOLUTION ELECTRON MICROSCOPY OF ANTIPHASE BOUNDARIES

Aberration corrected STEM images of an example of this kind of APB in $(Bi_{0.85}Nd_{0.15})(Ti_{0.1}Fe_{0.9})O_3$ along the [100] direction are shown in Fig. 1. These APBs lie on {100}

[a]Author to whom correspondence should be addressed. Electronic mail: ian.maclaren@glasgow.ac.uk

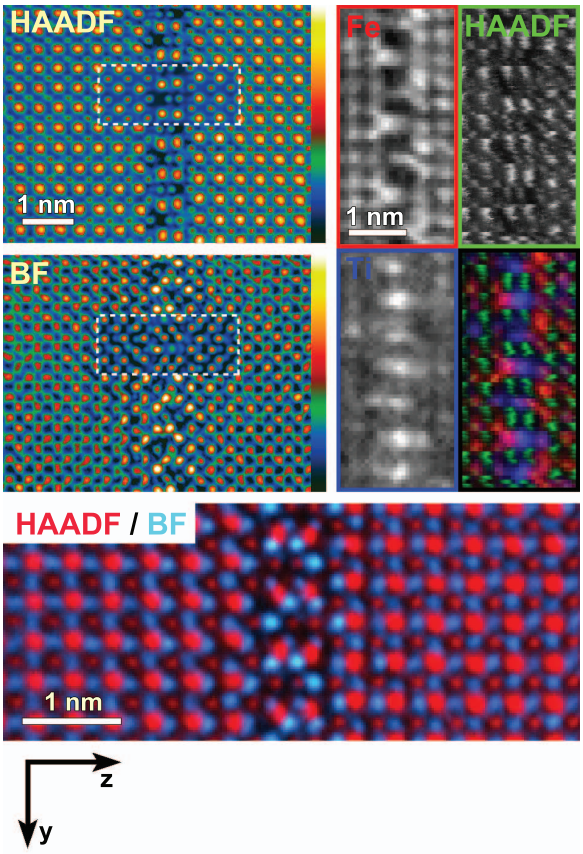

FIG. 1. Scanning transmission electron microscope images and EELS maps of the APB along the [100] projection; the colour scales are shown for the false colour images and the same scale was used for both HAADF and BF images. Insets of simulated images are overlaid on the experimental images using exactly the same contrast scale. The EELS maps for individual images show the full contrast range. In the RGB overlay of the Fe (R), HAADF (G), and Ti (B) signals, the contrast has been enhanced by removing the background intensity to improve visibility of the main atomic columns in the RGB image. The red/pale blue overlay image shows simultaneously acquired HAADF (red) and BF (pale blue) signals from an area of this APB and demonstrates the relative position of cations and anions in and around the boundary.

type planes of the pseudo-cubic perovskite structure. Here, we define the boundary plane as the (001) plane; the co-ordinate system is indicated in Fig. 1. The high angle annular dark field (HAADF) image shows brighter columns corresponding to the heavy Bi/Nd (A-site) ions and weaker columns corresponding to the lighter Fe/Ti (B-site) ions. It is clear from the HAADF image that there is a vertical shift of one half of a primitive perovskite unit cell across the boundary, as required for an APB. A key feature of the HAADF image is the "ladder" appearance of pairs of A-site ions in the boundary alternating with pairs of B-site ions along the vertical direction. A further feature of note in this image is the dark areas of contrast on alternate sides of the boundary in the vertical direction. The use of false colour scale allows subtle details of the low intensity part of the image to be readily seen in a way that would be difficult with a normal grey-scale image. Simultaneously with the HAADF, a bright field (BF) image was also recorded. This image shows clear atomic resolution contrast and it should be noted that the dark holes in the HAADF contrast correspond to bright areas in the BF image. Judging by the fact that the match to the contrast in simulations overlaid on the HAADF and BF images is the best for model thicknesses of 15.6 nm, we believe the sample to be about 16 nm thick in this region (although an uncertainty of 10%–20% about this figure would not be unreasonable). A part of the HAADF and BF images are also overlaid in a two colour red-cyan image and it is clear that the cyan-coloured BF image has bright areas where one would expect O-only columns in a ⟨100⟩ perovskite projections. LeBeau *et al.*[15] have definitively

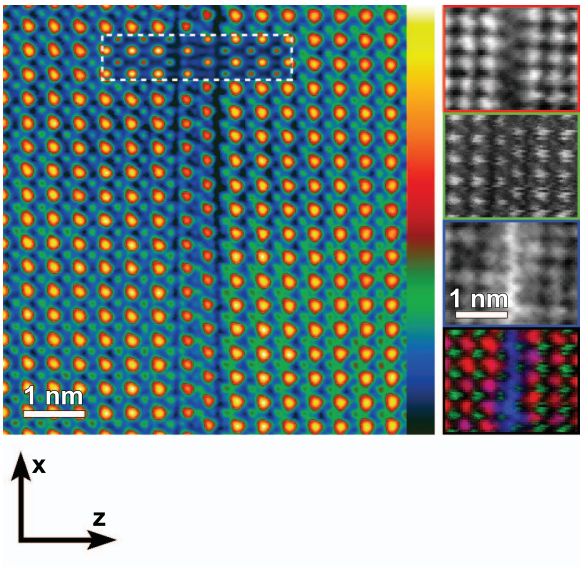

FIG. 2. HAADF image and EELS maps of the APB along the [010] projection, i.e., perpendicular to the projection in Fig. 1. An inset of a simulated image is overlaid on the HAADF image using exactly the same contrast scale. The EELS maps for individual images show the full contrast range. In the RGB overlay of the Fe (R), HAADF (G), and Ti (B) signals, the contrast has been enhanced by removing the background intensity to enhance visibility of the main atomic columns in the RGB image.

shown using a combination of experiment and simulation that O oxygen imaging can be formed for $SrTiO_3$ in exactly this fashion. For this reason, the O-ion positions in and around the boundary were interpreted as corresponding to the bright peaks in the BF image. Image simulations described in the supplementary material[28] support this interpretation and this is discussed more fully therein. A simulation of the BF image based on final atomic structure model (see below) is superimposed on the image in Fig. 1, and shows excellent agreement with the experimental image, confirming our identification of bright BF contrast with O positions in this structure.

To understand the chemistry in more detail, atomic resolution EELS was performed on one area of a boundary over an energy loss range from ∼250 eV to ∼1100 eV. Figure 1 shows maps of the Fe $L_{2,3}$ edge around 708 eV and the Ti $L_{2,3}$ edge around 456 eV. The Nd signal was also examined but little was found in the boundary, and only limited amounts were randomly distributed on A-site ion columns in the matrix to either side of the APB. The images indicate that the central B-site column is dominated by Ti with little Fe, additionally, there is a tendency for alternate columns to the left and right of the central Ti row to also contain some Ti. The HAADF signal, recorded simultaneously with the EELS signals (which mainly shows the heavy A-site atoms), is also shown in Fig. 1 together with a red-green-blue (RGB) image that simultaneously reveals the Fe (R), HAADF (G), and Ti (B) signals.

The same type of APB is shown in Fig. 2 but viewed from the perpendicular [010] direction. Figure 2 incorporates a HAADF image as well as atomic resolution EELS maps. A clear half unit cell shift in the vertical direction is once again observed across the boundary. The image is dominated by a shift of the bright A-site ion positions across the boundary, but a number of very weak B-site ion positions can also be distinguished as faint green dots using the false colour scale. Due to local mis-tilt and sample bending, the analysis of the corresponding BF image yielded a poorer accuracy on the O positions. Thanks to the high degree of redundancy in these experiments, this view was not used for the model building, but the image is presented in the supplementary material[28] for the interested reader. In agreement with the [100] projection shown in Fig. 1, there is evidence of deficiency and segregation of Fe and Ti, respectively, forming a corrugated sheet of Ti ions at the centre of the boundary.

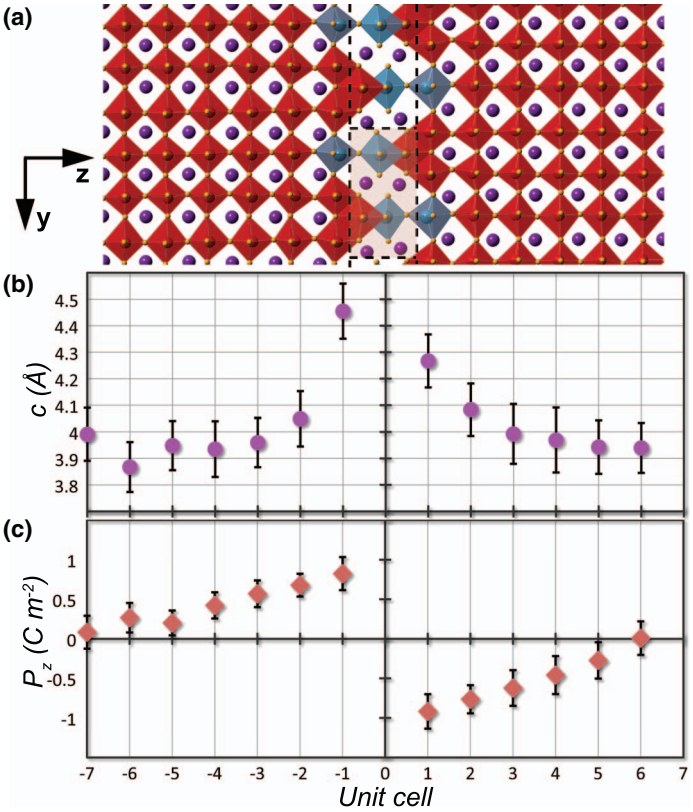

FIG. 3. Models and analysis of the APB: (a) [100] projection of the quantitative 3-dimensional structure of the APB (Fe – red, Ti – blue, Bi – purple, O – yellow); (b) The Bi-Bi plane spacing along the [001] direction as function of the distance from the boundary; (c) Local component of the polarisation in the [001], i.e., z direction as a function of distance from the boundary. The error bars in (b) and (c) were calculated from the standard deviation in the out-of-plane atomic position measurement after averaging.

RECONSTRUCTION OF THE 3D ATOMIC STRUCTURE

Positions of A- and B-site ions were measured quantitatively from the HAADF images shown in Figs. 1 and 2 using techniques described previously.[12,16] The positions of bright peaks in the bright field image of Fig. 1 were also determined in the same way and treated as representing O positions. Averaging was applied along the boundary in both cases to give confidence in the atom column position location and to allow a reasonable estimate of their accuracy. The two projections were then combined to yield a 3D atomic structure in a discrete tomography approach similar to that of Van Aert[17] and to previous work by one of the present authors.[18] It was assumed that the co-ordination to either side of the boundary was perovskite-like. With this assumption, the projected ionic positions in the boundary in the [100] and [010] projections can be correlated to obtain the 3D atomic positions of all atoms in the boundary. The [100] projection of the resulting 3D reconstruction is shown in Fig. 3(a) with a full crystallographic model available in supporting information. Errors on the position of A-, B-, and O-site ions were estimated as ~7 pm, 8 pm, and 10 pm, respectively. It should be noted that Nd-ions have not been included in the model, since they are isovalent, have a similar ionic radius and substitute randomly for Bi^{3+}. Similarly, away from the boundary, all B-sites are assumed to be Fe ions. It was also assumed that all O ions are displaced equally, both those visible in our BF images as separate columns and those present as mixed Fe-O columns. As may be seen in Fig. 3(a), all Fe and Ti atoms are co-ordinated octahedrally by 6 oxygens, although some octahedra close to or in the boundary are distorted with rather long Fe/Ti-O bond lengths. There is edge-sharing of some octahedra in the boundary giving a half-cell shift across the boundary in both the x and y directions, as required for an APB.

To validate the model, particularly with respect to the interpretation of the bright peaks in the bright field image as representing O columns, image simulations were performed using the QSTEM package.[19] Simulations were carried out at 100 kV, using 30 mrad convergence angle and a very small spherical aberration of -1 μm. The detectors were simulated for the parameters used in the SuperSTEM experiments, 0–5 mrad for the bright field detector and 100–170 mrad for the HAADF detector. Thicknesses of ~40 prototype perovskite unit cells (~15.5 nm) were used, with slices of half a cell and, in accordance with the frozen phonon method, an average of 30 phonon configurations were considered. The effects of a finite source size were taken into account by convolution of the simulated images with a 0.7 Å full-width at half-maximum Gaussian function. The results are overlaid on the experimental images in Figs. 1 and 2 and show excellent qualitative agreement with the 3D structure model in Fig. 3(a). In particular, the simulations confirm the identification of peaks in HAADF with cation positions and peaks in BF with oxygen anion positions, assuming full occupancy of these columns (fuller details are given in the supplementary material[28]). This is in good accord with previous work by LeBeau *et al.*[15] in which it was clearly demonstrated that BF image contrast in $SrTiO_3$ can result in peaks on the O ion columns under appropriate combinations of thickness and defocus.

LOCAL POLAR ORDER ADJACENT TO THE ANTIPHASE BOUNDARY

On inspection, the first layer of the model either side of the boundary is heavily distorted with respect to the antiferroelectric matrix with a much larger Bi-Bi spacing. The variation of the Bi-Bi plane spacing in the [001] direction was quantified and plotted as a function of distance from the APB centre, Fig. 3(b), and shows a peak value of ~4.4 Å in the unit cell immediately adjacent to the boundary, decaying in about 3–4 unit cells ~3.9 Å (the matrix value). Such highly distorted $BiFeO_3$ based unit cells have previously been seen in highly strained thin films[11,20] and around Nd-rich nanorods within the same ceramics.[16] Highly strained pseudotetragonal bismuth ferrite phases are typically associated with strong off-centring of the B-site ion and a large spontaneous polarisation (1.45 C m^{-2})[11,21] in comparison with, e.g., titanium rich lead zirconate titanate (0.8 C m^{-2}).[2] The present case is no exception and a large polarisation is visible in the overlay of HAADF and BF images (Fig. 1) where the O and Bi columns are displaced away and towards the boundary, respectively. From the quantitative displacement data in Fig. 3(b), and the resulting polarisation can be calculated using Born effective charges[2,12,22,23] and is shown in Fig. 3(c). It is noted that there is a slight asymmetry in the positions of the lighter ions with respect to the heavier ions across the whole image as has also been noted in previous work,[12,23] which probably arises from slight mistilt or residual aberration in the probe. This was symmetrised following a similar procedure to Lubk *et al.*[23] by shifting all Bi ions 10 pm to the left and all Fe/Ti ions 5 pm to the left with respect to the unshifted O positions to compensate for global shifts caused by a slight mistilt of the sample. A version of Fig. 3(c) calculated without using any shifts is included in the supplementary material.[28] The values are then slightly asymmetric, but the tendencies discussed below remain unchanged.

The out-of-plane polarisation shows a clear peak either side of the boundary to about 0.8–0.9 C m^{-2} and decays rapidly over about 5–6 unit cells to approximately zero. It should also be noted that the polarisation changes sign abruptly at the boundary. This all indicates that there is a strong E field radiating out from the boundary. The boundary area is marked with dotted lines in Fig. 3(a) and one repeat unit of the boundary is shown in a box. Within one perovskite unit cell thickness in this box there are 2 Ti^{4+} atoms, 2 Fe^{3+} atoms, 4 Bi^{3+} atoms, and 14 O^{2-} ions. Therefore, there is anion excess of two negative charge units within each cell resulting in a charge density on the APB of -0.68 C m^{-2}. The local field around the APB may in part be compensated by positive charge in the surrounding matrix from the substitution of Ti^{4+} ions onto Fe^{3+} sites. Nevertheless, the 3D structure model is consistent with polar order in the vicinity of the boundary, with an associated maximum polarisation near 1 C m^{-2}. This is in contrast with the bulk phase, which is known to have an antiferroelectric ordering.[16,24,25]

Note that, whilst all the analysis included in this paper is based on the images shown in Figures 1 and 2, quantitative evaluation of other images of similar antiphase boundaries in this ceramic showed

very similar trends in structure, out-of-plane lattice parameter and local polarisation and these are clearly a consistent feature of this composition.

Conventionally, an APB in an antiferroelectric matrix is expected to have a polarisation peak near the boundary because of uncompensated charge. In contrast, the structure reported here is effectively within a local paraelectric matrix with a strong polar order that decays within few unit cells of the APB. Furthermore, since the APB is a chemically segregated structure, it persists above any ferroelectric or antiferroelectric Curie temperature, and so presumably this local polar region will also persist to high temperature.

The gradual vanishing of the polarisation as one moves away from the APB suggests a combination of strain and electric fields that screen the excess charge at the APB over a range of unit cells. We suggest that the strain field created by the Ti-stabilised APB suppresses antiferroelectric (AFE) long range ordering, so that the region surrounding the APB is effectively a paraelectric. The charge trapped at the boundary is then screened by neighbouring polarisation resulting in the formation of a locally polar phase. This is very similar to the idea first put forward in the Heywang model of interface charge formation and its screening in bulk $BaTiO_3$.[26] In this model, the induced polarisation has a maximum value P_0 at the boundary, and according to the Poisson equation it will vary over the space charge region according to $dP/dx = e\, n_D$, where n_D is the bulk donor concentration. Using the estimates for P_0 obtained from the Born effective charge model, and the experimentally observed $d \sim 2.4$ nm, one arrives at a donor concentration of 2.6×10^{29} m^{-3}. This compares favourably with the unscreened 2 anions per unit cell value of 3.1×10^{29} m^{-3} indicating a good agreement between the excess charge at the boundary and the resulting polarisation of the surrounding material.

The final question of interest is why such an unlikely feature should form at all, when it imposes large elastic strains, produces significant local electric fields, and requires significant elemental segregation to take place at high temperature to allow its formation. This would all be energetically expensive and require a strong driving force; this is provided by the overdoping of the matrix with Ti. The target composition for the ceramic was $(Bi_{0.85}Nd_{0.15})(Ti_{0.1}Fe_{0.9})O_3$—as can be seen, the Ti^{4+} doping, will result in an excess positive charge into the matrix, which cannot be compensated by oxygen stoichiometry changes, as all oxygen sites are fully populated. Instead, we have already shown that one compensation mechanism is the formation of Nd-rich nanorod precipitates together with A-site vacancies.[16,27] Another possible mechanism is the exsolution of some of the excess Ti into Ti-rich features, such as the APBs studied in this work. It should be noted that nanorods are never observed within 5 unit cells of an APB, suggesting that compensation of excess Ti content by the formation of APBs takes away the driving force for the formation of the Nd-rich nanorods. Additionally, the formation of the negatively charged APBs will have an additional benefit for local charge balance since they will balance any tendency for the surrounding Ti-doped matrix to have an excess positive charge.

In summary, it has been shown that $(Bi_{0.85}Nd_{0.15})(Ti_{0.1}Fe_{0.9})O_3$ form highly unusual anion excess APBs with a structure unlike any previously observed in perovskites. The three dimensional structure of this boundary was recovered by combining HAADF and BF imaging from two orthogonal ⟨100⟩ projections to determine the ion positions, together with atomic resolution EELS. The reconstructed APB structure was used as an input for multislice frozen phonon simulations of the bright and dark field images which resulted in good qualitative agreement between simulations and experimental images, thereby validating positions and occupancies of O columns. The effect of this unusual APB on its surroundings is dramatic, causing a massive polarisation in ∼4–5 unit cells either side of the boundary obtaining peak values of ∼0.9 C m^{-2} within a local pseudotetragonal polar-ordered phase effectively embedded in a non-polar, orthorhombic, antiferroelectric matrix.

We gratefully acknowledge support by the EPSRC for the multiferroic ceramics work at Sheffield (EP/G069069/1 and EP/G005001/1), funding of the STEM work at SuperSTEM (EP/I000879/1 and EP/J009679/1), provision of a DTA studentship to L.Q.W., and ongoing support for the SuperSTEM facility. We are grateful to the Carnegie Trust for the Universities of Scotland for their provision of an Undergraduate Vacation Scholarship to O.M. We are also very thankful to Dr. Lothar Houben at the FZ-Jülich for the provision of the iMtools software used for the quantitative image analysis and

to Professor Christoph Koch at the University of Ulm for advice and help with the STEM image simulations using QSTEM.

[1] J. Seidel, L. W. Martin, Q. He, Q. Zhan, Y. H. Chu, A. Rother, M. E. Hawkridge, P. Maksymovych, P. Yu, M. Gajek, N. Balke, S. V. Kalinin, S. Gemming, F. Wang, G. Catalan, J. F. Scott, N. A. Spaldin, J. Orenstein, and R. Ramesh, Nature Mater. **8**, 229 (2009).
[2] C. L. Jia, S. B. Mi, K. Urban, I. Vrejoiu, M. Alexe, and D. Hesse, Nature Mater. **7**, 57 (2008).
[3] M. F. Chisholm, W. D. Luo, M. P. Oxley, S. T. Pantelides, and H. N. Lee, Phys. Rev. Lett. **105**, 197602 (2010).
[4] A. B. Shah, Q. M. Ramasse, S. J. May, J. Kavich, J. G. Wen, X. Zhai, J. N. Eckstein, J. Freeland, A. Bhattacharya, and J. M. Zuo, Phys. Rev. B **82**, 115112 (2010).
[5] A. B. Shah, Q. M. Ramasse, X. F. Zhai, J. G. Wen, S. J. May, I. Petrov, A. Bhattacharya, P. Abbamonte, J. N. Eckstein, and J. M. Zuo, Adv. Mater. **22**, 1156 (2010).
[6] P. Yu, J. S. Lee, S. Okamoto, M. D. Rossell, M. Huijben, C. H. Yang, Q. He, J. X. Zhang, S. Y. Yang, M. J. Lee, Q. M. Ramasse, R. Erni, Y. H. Chu, D. A. Arena, C. C. Kao, L. W. Martin, and R. Ramesh, Phys. Rev. Lett. **105**, 027201 (2010).
[7] C. L. Jia, V. Nagarajan, J. Q. He, L. Houben, T. Zhao, R. Ramesh, K. Urban, and R. Waser, Nature Mater. **6**, 64 (2007).
[8] H. J. Chang, S. V. Kalinin, A. N. Morozovska, M. Huijben, Y. H. Chu, P. Yu, R. Ramesh, E. A. Eliseev, G. S. Svechnikov, S. J. Pennycook, and A. Y. Borisevich, Adv. Mater. **23**, 2474 (2011).
[9] G. Catalan, A. Lubk, A. H. G. Vlooswijk, E. Snoeck, C. Magen, A. Janssen, G. Rispens, G. Rijnders, D. H. A. Blank, and B. Noheda, Nature Mater. **10**, 963 (2011).
[10] C. T. Nelson, B. Winchester, Y. Zhang, S. J. Kim, A. Melville, C. Adamo, C. M. Folkman, S. H. Baek, C. B. Eom, D. G. Schlom, L. Q. Chen, and X. Q. Pan, Nano Lett. **11**, 828 (2011).
[11] J. X. Zhang, Q. He, M. Trassin, W. Luo, D. Yi, M. D. Rossell, P. Yu, L. You, C. H. Wang, C. Y. Kuo, J. T. Heron, Z. Hu, R. J. Zeches, H. J. Lin, A. Tanaka, C. T. Chen, L. H. Tjeng, Y. H. Chu, and R. Ramesh, Phys. Rev. Lett. **107**, 147602 (2011).
[12] I. MacLaren, R. Villaurrutia, B. Schaffer, L. Houben, and A. Pelaiz-Barranco, Adv. Funct. Mater. **22**, 261 (2012).
[13] A. Y. Borisevich, A. R. Lupini, J. He, E. A. Eliseev, A. N. Morozovska, G. S. Svechnikov, P. Yu, Y. H. Chu, R. Ramesh, S. T. Pantelides, S. V. Kalinin, and S. J. Pennycook, Phys. Rev. B **86**, 140102 (2012).
[14] Y. M. Kim, A. Kumar, A. Hatt, A. N. Morozovska, A. Tselev, M. D. Biegalski, I. Ivanov, E. A. Eliseev, S. J. Pennycook, J. M. Rondinelli, S. V. Kalinin, and A. Y. Borisevich, Adv. Mater. **25**, 2497 (2013).
[15] J. M. LeBeau, A. J. D'Alfonso, S. D. Findlay, S. Stemmer, and L. J. Allen, Phys. Rev. B **80**, 174106 (2009).
[16] I. MacLaren, L. Q. Wang, B. Schaffer, Q. M. Ramasse, A. J. Craven, S. M. Selbach, N. A. Spaldin, S. Miao, K. Kalantari, and I. M. Reaney, Adv. Funct. Mater. **23**, 683 (2013).
[17] S. Van Aert, K. J. Batenburg, M. D. Rossell, R. Erni, and G. Van Tendeloo, Nature (London) **470**, 374 (2011).
[18] I. MacLaren and G. Richter, Philos. Mag. **89**, 169 (2009).
[19] C. Koch, Ph.D. thesis, Arizona State University, 2002.
[20] R. J. Zeches, M. D. Rossell, J. X. Zhang, A. J. Hatt, Q. He, C. H. Yang, A. Kumar, C. H. Wang, A. Melville, C. Adamo, G. Sheng, Y. H. Chu, J. F. Ihlefeld, R. Erni, C. Ederer, V. Gopalan, L. Q. Chen, D. G. Schlom, N. A. Spaldin, L. W. Martin, and R. Ramesh, Science **326**, 977 (2009).
[21] A. J. Hatt, N. A. Spaldin, and C. Ederer, Phys. Rev. B **81**, 054109 (2010).
[22] D. Kan, L. Palova, V. Anbusathaiah, C. J. Cheng, S. Fujino, V. Nagarajan, K. M. Rabe, and I. Takeuchi, Adv. Funct. Mater. **20**, 1108 (2010).
[23] A. Lubk, M. D. Rossell, J. Seidel, Q. He, S. Y. Yang, Y. H. Chu, R. Ramesh, M. J. Hytch, and E. Snoeck, Phys. Rev. Lett. **109**, 047601 (2012).
[24] S. Karimi, I. M. Reaney, I. Levin, and I. Sterianou, Appl. Phys. Lett. **94**, 112903 (2009).
[25] K. Kalantari, I. Sterianou, D. C. Sinclair, P. A. Bingham, J. Pokorny, and I. M. Reaney, J. Appl. Phys. **111**, 064107 (2012).
[26] W. Heywang, J. Mater. Sci. **6**, 1214 (1971).
[27] I. M. Reaney, I. MacLaren, L. Q. Wang, B. Schaffer, A. Craven, K. Kalantari, I. Sterianou, S. Karimi, and D. C. Sinclair, Appl. Phys. Lett. **100**, 182902 (2012).
[28] See supplementary material at http://dx.doi.org/10.1063/1.4818002 for sample preparation and microscopy experimental details, a fuller discussion of oxygen position determination with the aid of image simulations, full details of the reconstruction of the 3D structure and the calculation of the polarisation variation with position, and the final validation of the model using image simulations, as well as a full xyz model of the 3D atomic structure for viewing in a range of crystal and molecule viewers.